

Steep-slope Schottky diode with cold metal source

Cite as: Appl. Phys. Lett. **120**, 243506 (2022); <https://doi.org/10.1063/5.0097408>

Submitted: 28 April 2022 • Accepted: 06 June 2022 • Published Online: 15 June 2022

 Wongil Shin, Gyuho Myeong, Kyunghwan Sung, et al.



View Online



Export Citation



CrossMark

 QBLOX



1 qubit

Shorten Setup Time

Auto-Calibration

More Qubits

Fully-integrated

Quantum Control Stacks

Ultrastable DC to 18.5 GHz

Synchronized <<1 ns

Ultralow noise



100s qubits

visit our website >

Steep-slope Schottky diode with cold metal source

Cite as: Appl. Phys. Lett. **120**, 243506 (2022); doi: [10.1063/5.0097408](https://doi.org/10.1063/5.0097408)

Submitted: 28 April 2022 · Accepted: 6 June 2022 ·

Published Online: 15 June 2022



View Online



Export Citation



CrossMark

Wongil Shin,¹ Gyuho Myeong,¹ Kyunghwan Sung,¹ Seungho Kim,¹ Hongsik Lim,¹ Boram Kim,¹ Taehyeok Jin,¹ Jihoon Park,¹ Kenji Watanabe,² Takashi Taniguchi,² Fei Liu,^{3,a)} and Sungjae Cho^{1,a)}

AFFILIATIONS

¹Department of Physics, Korea Advanced Institute of Science and Technology (KAIST), Daejeon, Republic of Korea

²National Institute for Materials Science, Namiki, Tsukuba, Ibaraki 305-0044, Japan

³School of Integrated Circuits, Peking University, Beijing 100871, China

^{a)}Authors to whom correspondence should be addressed: feiliu@pku.edu.cn and sungjae.cho@kaist.ac.kr

ABSTRACT

Today's circuit technology requires low-power transistors and diodes to extend Moore's law. While research has been focused on reducing power consumption of transistors, low-power diodes have not been widely studied. Here, we report a low-power, thus steep-slope Schottky diode, with a "cold metal" source. The Schottky barrier between metal electrode and bulk MoS₂ enabled the diode behavior, and the steep-slope diode IV curve originated from the change in the density of states of a graphite (cold metal) source with a bias voltage. The MoS₂ Schottky diode with a cold metal exhibits an ideality factor (η) < 1 for more than four decades of drain current with a sizable rectifying ratio (10^8). The realization of a steep-slope Schottky diode paves the way to the improvement in low-power circuit technology.

© 2022 Author(s). All article content, except where otherwise noted, is licensed under a Creative Commons Attribution (CC BY) license (<http://creativecommons.org/licenses/by/4.0/>). <https://doi.org/10.1063/5.0097408>

Two-dimensional (2D) van der Waals (vdW) materials are known as potential candidates for use as next-generation devices because of their unique electronic and optoelectronic properties.^{1–8} Monolayer (ML) transition metal dichalcogenides (TMDC), such as WS₂, WSe₂, MoSe₂, and MoS₂, are being widely used to develop electronic devices, including field-effect transistors (FETs), diodes, and sensors, since they have suitable bandgap and high carrier mobility.^{9–17} Among TMDCs, the monolayer MoS₂ is most frequently used in developing electronic devices owing to its high carrier mobility (>200 cm²/V s).^{17–20} However, the formation of defects and impurities during the metal deposition process at the metal–semiconductor interface is a bottleneck for improving device performance.^{21–23}

Because electronic miniaturization and Moore's law are approaching their limit, reducing the energy consumption of electronic devices has drawn significant attention.^{24,25} To reduce energy consumption, the thermionic limit of the transistor with subthreshold swing (SS) = 60 mV/dec has been overcome by proposing alternate transistors, such as the tunnel field-effect transistor (TFET), the negative capacitance field-effect transistor (NC-FET), and the Dirac-source field-effect transistor (DS-FET).^{26–41} However, the steep-slope diode has not been studied widely although diodes are key electronic components along with transistors.

In this work, we report a steep-slope MoS₂ Schottky diode with a sub-unity ideality factor. The ideality factor (η) represents the steepness of the drain current increase with the bias voltage. The ideality factor η can be obtained from the Schottky diode equation,

$$I_D = I_S(1 - e^{qV_D/\eta k_B T}), \quad (1)$$

where I_D and I_S are the drain and saturation current, respectively. By using cold metal (graphite) as a source electrode in our MoS₂ Schottky diode, we achieved a sub-unity ideality factor for more than four decades of drain current with a sizable rectifying ratio ($I_{on}/I_{off} > 10^8$). In contrast to the constant density of states in a regular metallic material, graphite has an abrupt change in density of states near charge neutrality points, which results in a super-exponentially decaying carrier density with energy (see [supplementary material S1](#)).

Figures 1(a)–1(c) show the optical and schematic image of our MoS₂ diode consisting of four components: (i) graphite contact on a monolayer MoS₂ with a monolayer hexagonal boron nitride (hBN) spacer between them, (ii) monolayer MoS₂ channel, (iii) bulk MoS₂ drain with direct metal (chromium/gold, Cr/Au) contact, and (iv) top, control (chromium/gold, Cr/Au), and back (platinum, Pt) gate electrodes. To avoid air exposure and oxidation of the MoS₂ monolayer,

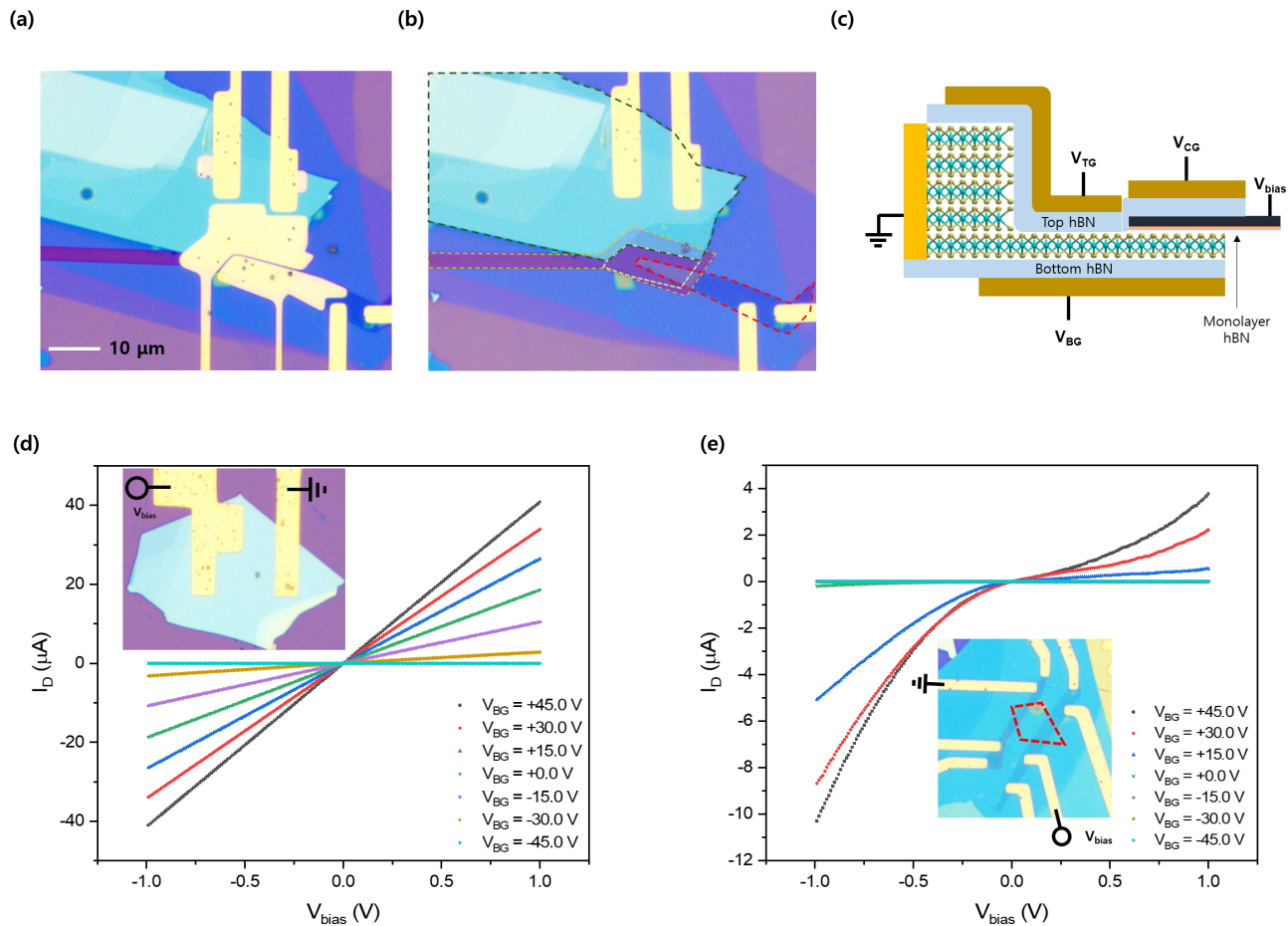


FIG. 1. (a) Optical image of fabricated cold metal source device. (b) Red, light green, and dark green dashed lines indicate graphite, monolayer MoS₂, and bulk MoS₂, respectively. To prevent contamination with chemicals and oxygens, we fully encapsulate the heterostructure with ~ 10 nm thickness of top and bottom hBN. Yellow dashed line indicates platinum backgate. We used graphite contact with monolayer hBN as a source and metal contacts on bulk MoS₂ as a drain. (c) Schematic of the cold metal source device. There are three kinds of gate. The topgate is placed on the channel MoS₂, and it controls the Fermi level of the channel. The control gate is placed on the graphite contact, and it can control the Fermi level of graphite contact. At last, the backgate is placed under the monolayer MoS₂ region, and it controls the Fermi level of part of graphite contact as well as the monolayer MoS₂ channel. (d) Ohmic contact behavior of two graphite contacts with monolayer hBN on monolayer MoS₂. According to any gate voltages, the characteristic I_D - V_{bias} curves show Ohmic behavior. (e) Non-Ohmic contact behavior of two metal contact on bulk MoS₂. All the characteristic I_D - V_{bias} curves show non-Ohmic contact with a full range of V_{BG} . Insets of Figs. 1(d) and 1(e) show the measured device (see [supplementary material S4](#)).

we mechanically exfoliate the MoS₂, stack the vdW heterostructures via the dry transfer method,^{28,42,43} and encapsulate them using hBN inside an N₂-filled glovebox (see [supplementary material S2](#)). We used Raman spectra measurements to confirm the number of layers in MoS₂ flakes (see [supplementary material S3](#)).^{44,45} We also used a monolayer MoS₂ connected naturally with bulk MoS₂. Since direct metal deposition may cause damage and change the electronic property of monolayer MoS₂, we contacted the monolayer MoS₂ using monolayer hBN/graphite at the source side and Cr/Au metal deposition on the bulk MoS₂ (naturally connected to the monolayer MoS₂) at the drain side. [Figure 1\(c\)](#) shows the device schematic, and there are three kinds of gate electrodes—platinum backgate (BG), control gate (CG), and topgate (TG). The role of each gate is little bit different. By controlling the backgate, the Fermi level of monolayer MoS₂ and that of part of graphite contact are raised or lowered. The control gate can change the Fermi level of graphite

contact. In this experiment, we make the graphite contact p-type or n-type by controlling this control gate. At last, the topgate controls the Fermi level of the channel MoS₂. We used monolayer hBN to form Ohmic contact between graphite and monolayer MoS₂. We fabricated additional devices to investigate the properties of our electrodes (see [supplementary material S4](#)). [Figure 1\(d\)](#) shows the IV curves of a MoS₂ monolayer in contact with monolayer hBN/graphite electrodes, while [Fig. 1\(e\)](#) shows IV curves of bulk MoS₂ in contact with the Cr/Au metal. The MoS₂ device in contact with the monolayer MoS₂/graphite shows linear IV curves at all gate voltages, indicating Ohmic contact formation. On the other hand, bulk MoS₂ in contact with the Cr/Au metal shows nonlinear IV curves, which prove Schottky contact (see [supplementary material S5 and S6](#)).^{21,46–54}

[Figure 2\(a\)](#) presents the drain current (I_D) vs bias voltage (V_{bias}) curves of the MoS₂ Schottky diode at $V_{\text{BG}} = -1.0$ V, $V_{\text{TG}} = +0.5$ V,

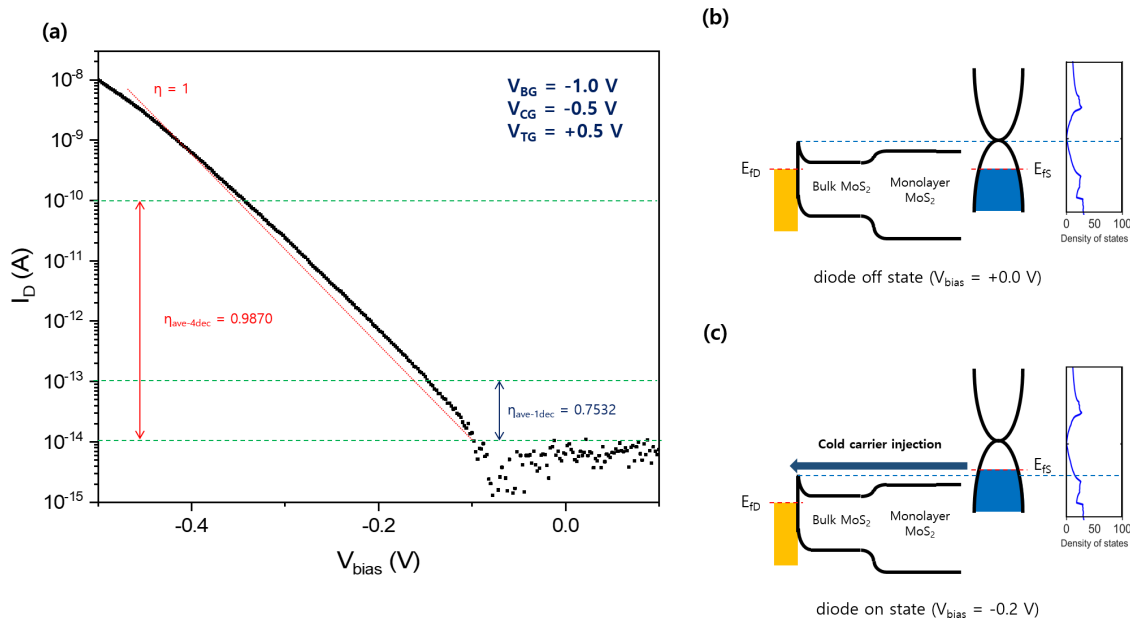


FIG. 2. (a) Characteristic I_D - V_{bias} curve at $V_{\text{BG}} = -1.0$ V, $V_{\text{CG}} = -0.5$ V, and $V_{\text{TG}} = +0.5$ V. Ideality factor below unity keeps for 4 decades, and ideality factor for 1 decade is 0.7532. (b) Band diagram of the diode off-state. (c) Band diagram of the diode-on state with cold carrier injection from graphite contact.

and $V_{\text{CG}} = -0.5$ V, where the graphite electrode is p-type. Figures 2(b) and 2(c) show the corresponding band diagrams at the forward and reverse bias voltage (on- and off-state). Note that the density of states in graphite changes significantly near the charge neutrality point. As the drain bias voltage applied to the graphite decreases negatively from the off-state, a forward bias is applied with on-current flowing through the channel, which indicates that the Schottky barrier at the interface between the metal contact and n-type MoS_2 dominates the diode operation. When a negative bias voltage $V_{\text{bias}} < 0$ is applied to graphite, the electrochemical potential of the graphite electrode is increased by eV_{bias} with respect to that of the metal contact. It is noteworthy that the electrons in the graphite source contributing to the current injection should have energy between E_F in graphite and the green dotted line in the band diagram, which is determined by the bulk MoS_2 conduction band edge. As the $V_{\text{bias}} < 0$ increases in the positive direction from the on- to off-state, the electrochemical potential of graphite decreases with the energy crossing the band edge of graphite moving closer to the charge neutrality point (CNP). In this case, due to the reduced graphite density of state (DOS) from the on- to off-state (thereby super-exponential decrease in carrier density of the graphite source), the IV curves from the on- to off-state become steeper than the conventional Schottky diode, and the ideality factor becomes less than unity at room temperature. Figures 3(a) and 3(b) show the control gate-dependent diode characteristic curve and ideality factor $\eta_{\text{ave-1dec}}$. The ideality factor $\eta_{\text{ave-1dec}}$ becomes less than unity only when graphite is p-type. When graphite is n-type, the ideality factor $\eta_{\text{ave-1dec}}$ becomes greater than unity as in conventional Schottky diode.

Monolayer graphene has a linear density of states to filter high energy electrons and, thus, has been applied to realize steep slope DS FETs and diodes. Can graphite be applied as a cold electron injection source to realize steep switching similarly? To address this question

theoretically, we compared transmissions of monolayer graphene and graphite as shown in Fig. 4(a), which are calculated by atomistic quantum transport simulations based on the density functional theory coupled with nonequilibrium Green's function (NEGF) theory implemented in the Nanodcal package.⁵⁵ Intrinsic monolayer graphene has massless Dirac electrons and a linear energy dispersion around the Fermi level. Therefore, the transmission of monolayer graphene linearly depends on energy. Electrons in graphite are no longer massless and have finite states at the Fermi level. Even though graphite does not have a linear energy dispersion, transmission monotonically increases with the energy difference with respect to the Fermi level, which is similar to that of graphene as shown in Fig. 4(a). Switching properties of the graphite- MoS_2 diode as shown in Fig. 4(b) can be estimated by Landauer-Büttiker formula,⁵⁶

$$I = \frac{2e}{h} \int_{E_{\text{top}}}^{\infty} T(E) (f_L(E - E_{FL}) - f_R(E - E_{FR})) dE, \quad (2)$$

where E_{top} is the top of channel barrier, $f_{L/R}$ is the Fermi distribution function of left/right lead, and E_{FL} and E_{FR} are the Fermi levels of left and right leads, respectively. Figure 4(c) shows I_D vs V_D of the graphite- MoS_2 diode with a p-type graphite. It is found that the ideality factor is smaller than 1 as $-0.52 \text{ V} < V_D < -0.32 \text{ V}$, and the minimum value reaches 0.73. In the bias voltage region, current is increased by four orders of magnitude. The reason for such steep switching is that high energy electrons are partly filtered as the top of channel barrier around the intrinsic Fermi level of graphite as shown in Fig. 4(d). As the diode is switched from the off- to on-state as shown in Fig. 4(d), the injected electron density of states around the top of channel barrier is increased simultaneously, which is different from conventional metal with constant DOS and makes the diode switch much faster than the conventional Schottky diode.

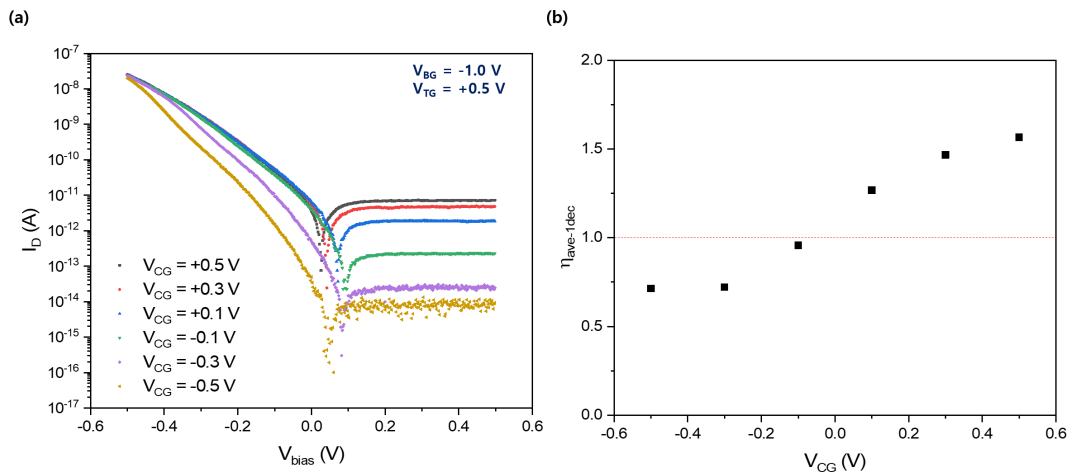


FIG. 3. (a) Characteristic I_D vs V_{bias} curves at different control gate voltage. Under $V_{CG} < 0$ V, characteristic curves show steep-slope behavior. (b) V_{CG} vs ideality factor (average over one decade). For $V_{CG} \leq +0.0$ V, the ideality factor remained below unity for one decade.

In summary, we develop a steep-slope Schottky diode with cold carrier injection consisting of monolayer MoS_2 naturally connected to bulk MoS_2 and graphite cold metal contact. The results demonstrated that using cold metal sources increases the Schottky diode switching slope. As the cold carrier injected from the cold metal source

(graphite), the Schottky diode exhibits an unconventional ideality factor of (η) < 1 for more than three decades of drain current with a sizeable rectifying ratio ($\sim 10^8$) (see [supplementary material S9](#)). Our demonstration of the steep-slope Schottky diode paves the way to achieving low-power circuit technology requiring rectifiers.

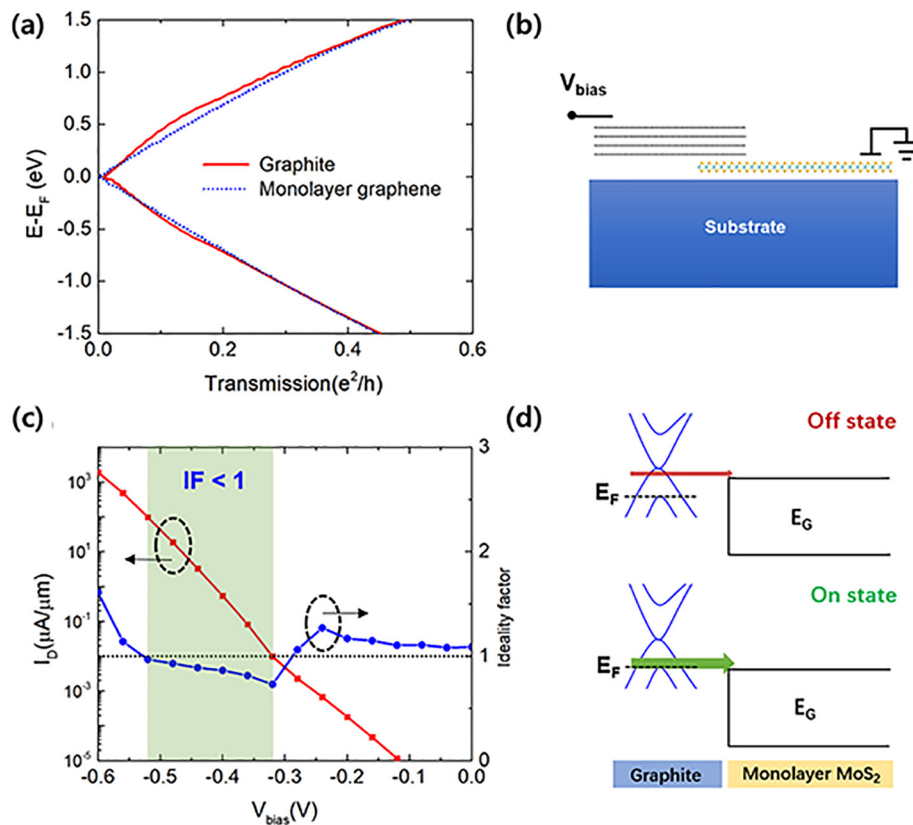


FIG. 4. (a) Transmissions of graphite and monolayer graphene obtained by first-principles quantum transport simulations. The transmission of graphite is normalized to the monolayer. (b) Simulation model for the steep slope diode with the cold metal source of graphite. V_{bias} is applied to graphite contact, and the graphite contact is on the monolayer MoS_2 channel. (c) I_D - V_{bias} curve and ideality factor of the graphite- MoS_2 diode with p-type graphite by theoretical calculations. (d) Band diagram for the graphite- MoS_2 diode with p-type graphite at on- and off-states.

See the [supplementary material](#) for more details regarding the manuscript.

S.C. acknowledges support from National Research Foundation of Korea (Grant Nos. 2020M3F3A2A01081899 and 2020R1A2C2100258). F.L. acknowledges support from National Science Foundation of China (Grant No. 61974003) and the 111 Project (Grant No. B18001).

AUTHOR DECLARATIONS

Conflict of Interest

The authors have no conflicts to disclose.

Author Contributions

Wongil Shin: Data curation (equal); Investigation (equal); Methodology (equal); Writing – original draft (equal); Writing – review and editing (equal). **Gyuhoo Myeong:** Data curation (equal); Investigation (equal); Methodology (equal); Writing – original draft (equal). **Kyunghwan Sung:** Data curation (supporting); Investigation (supporting); Methodology (supporting). **Seungho Kim:** Data curation (supporting); Investigation (supporting); Methodology (supporting). **Hongsik Lim:** Data curation (supporting). **Boram Kim:** Data curation (supporting). **Taehyeok Jin:** Data curation (supporting). **Jihoon Park:** Data curation (supporting). **Kenji Watanabe:** Resources (equal). **Takashi Taniguchi:** Resources (equal). **Fei Liu:** Formal analysis (equal); Writing – original draft (equal). **Sungjae Cho:** Conceptualization (equal); Formal analysis (equal); Funding acquisition (equal); Project administration (equal); Supervision (equal); Writing – original draft (equal); Writing – review and editing (equal).

DATA AVAILABILITY

The data that support the findings of this study are available within the article and its [supplementary material](#).

REFERENCES

- K. S. Novoselov, V. I. Fal'ko, L. Colombo, P. R. Gellert, M. G. Schwab, and K. Kim, *Nature* **490**, 192 (2012).
- N. O. Weiss, H. Zhou, L. Liao, Y. Liu, S. Jiang, Y. Huang, and X. Duan, *Adv. Mater.* **24**, 5782 (2012).
- Q. H. Wang, K. Kalantar-Zadeh, A. Kis, J. N. Coleman, and M. S. Strano, *Nat. Nanotechnol.* **7**, 699 (2012).
- G. Konstantatos, M. Badioli, L. Gaudreau, J. Osmond, M. Bernechea, F. P. G. De Arquer, F. Gatti, and F. H. L. Koppens, *Nat. Nanotechnol.* **7**, 363 (2012).
- A. K. Geim and I. V. Grigorieva, *Nature* **499**, 419 (2013).
- M. Chhowalla, H. S. Shin, G. Eda, L. J. Li, K. P. Loh, and H. Zhang, *Nat. Chem.* **5**, 263 (2013).
- S. Kar, J. Lake, S. O. Adeyemo, T. S. Santra, and H. J. Joyce, *Mater. Today Phys.* **23**, 100631 (2022).
- Z. Zheng, X. Zu, Y. Zhang, and W. Zhou, *Mater. Today Phys.* **15**, 100262 (2020).
- B. Radisavljevic and A. Kis, *Nat. Mater.* **12**, 815 (2013).
- H. C. P. Movva, A. Rai, S. Kang, K. Kim, B. Fallahazad, T. Taniguchi, K. Watanabe, E. Tutuc, and S. K. Banerjee, *ACS Nano* **9**, 10402 (2015).
- N. R. Pradhan, D. Rhodes, S. Memaran, J. M. Poumirol, D. Smirnov, S. Talapatra, S. Feng, N. Perea-Lopez, A. L. Elias, M. Terrones, P. M. Ajayan, and L. Balicas, *Sci. Rep.* **5**, 8979 (2015).
- J. S. Rhyee, J. Kwon, P. Dak, J. H. Kim, S. M. Kim, J. Park, Y. K. Hong, W. G. Song, I. Omkaram, M. A. Alam, and S. Kim, *Adv. Mater.* **28**, 2316 (2016).
- S. Manzeli, D. Ovchinnikov, D. Pasquier, O. V. Yazyev, and A. Kis, *Nat. Rev. Mater.* **2**, 17033 (2017).
- A. S. Aji, P. Solís-Fernández, H. G. Ji, K. Fukuda, and H. Ago, *Adv. Funct. Mater.* **27**, 1703448 (2017).
- G. Luo, Z. Z. Zhang, H. O. Li, X. X. Song, G. W. Deng, G. Cao, M. Xiao, and G. P. Guo, *Front. Phys.* **12**, 128502 (2017).
- S. Kim, A. Konar, W. S. Hwang, J. H. Lee, J. Lee, J. Yang, C. Jung, H. Kim, J. B. Yoo, J. Y. Choi, Y. W. Jin, S. Y. Lee, D. Jena, W. Choi, and K. Kim, *Nat. Commun.* **3**, 1011 (2012).
- X. Cui, G. H. Lee, Y. D. Kim, G. Arefe, P. Y. Huang, C. H. Lee, D. A. Chenet, X. Zhang, L. Wang, F. Ye, F. Pizzocchero, B. S. Jessen, K. Watanabe, T. Taniguchi, D. A. Muller, T. Low, P. Kim, and J. Hone, *Nat. Nanotechnol.* **10**, 534 (2015).
- D. Lembke and A. Kis, *ACS Nano* **6**, 10070 (2012).
- T. Shen, F. Li, L. Xu, Z. Zhang, F. Qiu, Z. Li, and J. Qi, *J. Mater. Sci.* **55**, 14315 (2020).
- J. Wang, Q. Yao, C. W. Huang, X. Zou, L. Liao, S. Chen, Z. Fan, K. Zhang, W. Wu, X. Xiao, C. Jiang, and W. W. Wu, *Adv. Mater.* **28**, 8302 (2016).
- Y. Liu, J. Guo, E. Zhu, L. Liao, S. J. Lee, M. Ding, I. Shakir, V. Gambin, Y. Huang, and X. Duan, *Nature* **557**, 696 (2018).
- Y. Jung, M. S. Choi, A. Nipane, A. Borah, B. Kim, A. Zangibadi, T. Taniguchi, K. Watanabe, W. J. Yoo, J. Hone, and J. T. Teherani, *Nat. Electron.* **2**, 187 (2019).
- B. Yarrow, A. M. Askar, A. M. Parameswaran, and M. M. Adachi, *ACS Appl. Electron. Mater.* **1**, 2150 (2019).
- C. A. MacK, *IEEE Trans. Semicond. Manuf.* **24**, 202 (2011).
- E. Pop, *Nano Res.* **3**, 147 (2010).
- D. Sarkar, X. Xie, W. Liu, W. Cao, J. Kang, Y. Gong, S. Kraemer, P. M. Ajayan, and K. Banerjee, *Nature* **526**, 91 (2015).
- S. Kim, G. Myeong, W. Shin, H. Lim, B. Kim, T. Jin, S. Chang, K. Watanabe, T. Taniguchi, and S. Cho, *Nat. Nanotechnol.* **15**, 203 (2020).
- M. Liu, H. N. Jaiswal, S. Shahi, S. Wei, Y. Fu, C. Chang, A. Chakravarty, X. Liu, C. Yang, Y. Liu, Y. H. Lee, V. Perebeinos, F. Yao, and H. Li, *ACS Nano* **15**, 5762 (2021).
- X. Yan, C. Liu, C. Li, W. Bao, S. Ding, D. W. Zhang, and P. Zhou, *Small* **13**, 1701478 (2017).
- E. Norouzzadeh, S. Mohammadi, and M. Moradinasab, *Mater. Sci. Semicond. Process.* **138**, 106258 (2022).
- K. Jang, T. Saraya, M. Kobayashi, and T. Hiramoto, *Solid. State. Electron.* **136**, 60 (2017).
- S. B. Rahi, S. Tayal, and A. K. Upadhyay, *Microelectron. J.* **116**, 105242 (2021).
- R. Gandhi, Z. Chen, N. Singh, K. Banerjee, and S. Lee, *IEEE Electron Device Lett.* **32**, 1504 (2011).
- S. Kim, G. Myeong, J. Park, K. Watanabe, T. Taniguchi, and S. Cho, *Nano Lett.* **20**, 3963 (2020).
- J. Xu, J. Jia, S. Lai, J. Ju, and S. Lee, *Appl. Phys. Lett.* **110**, 033103 (2017).
- W. G. Vandenberghe, A. S. Verhulst, B. Sorée, W. Magnus, G. Groeseneken, Q. Smets, M. Heyns, and M. V. Fischetti, *Appl. Phys. Lett.* **102**, 013510 (2013).
- A. M. Ionescu and H. Riel, *Nature* **479**, 329 (2011).
- X. Wang, P. Yu, Z. Lei, C. Zhu, X. Cao, F. Liu, L. You, Q. Zeng, Y. Deng, C. Zhu, J. Zhou, Q. Fu, J. Wang, Y. Huang, and Z. Liu, *Nat. Commun.* **10**, 3037 (2019).
- C. Qiu, F. Liu, L. Xu, B. Deng, M. Xiao, J. Si, L. Lin, Z. Zhang, J. Wang, H. Guo, H. Peng, and L. M. Peng, *Science* **361**, 387 (2018).
- M. Xiao, Y. Lin, L. Xu, B. Deng, H. Peng, L. M. Peng, and Z. Zhang, *Adv. Electron. Mater.* **6**, 2000258 (2020).
- Z. Tang, C. Liu, X. Huang, S. Zeng, L. Liu, J. Li, Y. G. Jiang, D. W. Zhang, and P. Zhou, *Nano Lett.* **21**, 1758 (2021).
- K. Kinoshita, R. Moriya, M. Onodera, Y. Wakafuji, S. Masubuchi, K. Watanabe, T. Taniguchi, and T. Machida, *Npj 2D Mater. Appl.* **3**, 22 (2019).
- F. Pizzocchero, L. Gammelgaard, B. S. Jessen, J. M. Caridad, L. Wang, J. Hone, P. Bøggild, and T. J. Booth, *Nat. Commun.* **7**, 11894 (2016).
- H. Li, Q. Zhang, C. C. R. Yap, B. K. Tay, T. H. T. Edwin, A. Olivier, and D. Baillargeat, *Adv. Funct. Mater.* **22**, 1385 (2012).
- L. Liang and V. Meunier, *Nanoscale* **6**, 5394 (2014).
- J. Y. Wu, Y. T. Chun, S. Li, T. Zhang, and D. Chu, *ACS Appl. Mater. Interfaces* **10**, 24613 (2018).

- ⁴⁷E. Pollmann, S. Slezione, T. Foller, U. Hagemann, C. Gorynski, O. Petri, L. Madauß, L. Breuer, and M. Schleberger, *ACS Omega* **6**, 15929 (2021).
- ⁴⁸J. Kwon, J. Y. Lee, Y. J. Yu, C. H. Lee, X. Cui, J. Hone, and G. H. Lee, *Nanoscale* **9**, 6151 (2017).
- ⁴⁹D. Qiu and E. K. Kim, *Sci. Rep.* **5**, 13743 (2015).
- ⁵⁰C. Kim, I. Moon, D. Lee, M. S. Choi, F. Ahmed, S. Nam, Y. Cho, H. J. Shin, S. Park, and W. J. Yoo, *ACS Nano* **11**, 1588 (2017).
- ⁵¹Z. Wang, X. Xiong, J. Li, and M. Dong, *Mater. Today Phys.* **16**, 100290 (2021).
- ⁵²F. Giannazzo, G. Fisichella, A. Piazza, S. D. Franco, I. P. Oliveri, S. Agnello, and F. Roccaforte, *Mater. Sci. Semicond. Process.* **42**, 174 (2016).
- ⁵³C. Maurel, F. Ajuston, R. Péchou, G. Seine, and R. Coratger, *Surf. Sci.* **600**, 442 (2006).
- ⁵⁴A. Allain, J. Kang, K. Banerjee, and A. Kis, *Nat. Mater.* **14**, 1195 (2015).
- ⁵⁵J. Taylor, H. Guo, and J. Wang, *Phys. Rev. B.* **63**, 245407 (2001).
- ⁵⁶S. Datta, *Quantum Transport: Atom to Transistor* (Cambridge University Press, Cambridge, 2005).